2024 EC³
2024 European Conference on Computing in Construction
Chania, Crete, Greece
July 15-17, 2024

TOWARDS DETECTING DAMAGE IN LIGHTWEIGHT BRIDGES WITH TRAVELING MASSES USING MACHINE LEARNING

Georgios Dadoulis[1], George D. Manolis[1], Konstantinos Katakalos[1], Thamer Al-Zuriqat[2], Kosmas Dragos[2], and Kay Smarsly[2]
[1]Aristotle University of Thessaloniki, Thessaloniki, Greece
[2]Hamburg University of Technology, Hamburg, Germany

Abstract

Lightweight bridges are subjected to moving loads (vehicular traffic), with vehicular masses typically being comparable to structural masses. Moving loads are thus regarded as "traveling masses", resulting in complex dynamic behavior, which is hardly covered by conventional damage detection strategies. This paper presents a concept towards damage detection in lightweight bridges with traveling masses using machine learning (ML). Specifically, a ML model for classifying structural damage is trained, using simulations, and applied using real-world structural response data. Preliminary tests of the proposed concept validate the power of the ML model in identifying structural damage, despite the non-stationarity of the problem.

Introduction

Research on advancing material technologies to develop high-strength materials has been conducted since the second half of the 20th century (Flaga, 2000). The construction industry has been increasingly leveraging high-strength materials in an attempt to meet structural design requirements while reducing material usage (Zhang et al., 2019). Furthermore, in bridge design and construction, practitioners frequently seek to reduce the size of structural elements, which, apart from the obvious financial benefit, also helps meet practical and aesthetical requirements.

High-strength materials, however, frequently result in lightweight flexible structures, which are prone to heavy oscillations. A notable example is the case of the Millennium Bridge in London, which exhibited large oscillations, due to the large crowds drawn during opening in 2000 (Dallard et al., 2001). Consequently, material reduction in bridges requires care to avoid unanticipated oscillations. Moreover, placing the discussion on bridge oscillations under operational conditions, bridges are expected to withstand oscillations induced by operational loads, such as vehicular traffic.

At a first glance, the problem of vehicles traversing bridge decks may be described as a "moving load" problem, the dynamics of which differ from conventional structural dynamics, in that the structural response is affected by the velocity of the vehicles (Firus, 2023). In lightweight bridges, however, vehicular masses may be comparable to structural masses (particularly in railway bridges) and are regarded as "traveling masses", resulting in a complex non-stationary problem. With respect to damage detection, which is the focal point of structural maintenance, conventional damage detection strategies hardly address the traveling-mass problem. Experimental techniques as well as structural health monitoring (SHM) strategies typically rely on data analysis methods suitable for stationary problems, e.g. identifying the frequency content of structural response data using the Fourier transform (Dragos et al., 2024). Studies on moving loads on beams also fail to capture the damage-detection traveling-mass problem in its totality.

Approaches describing the dynamic response of beam structures under traveling masses have been widespread in literature. Examples range from as far back as the late 1990s, with the work of Siddiqui et al. (1998) who investigated the motion of a cantilever Euler-Bernoulli beam under the effect of a moving mass-spring system, to recent works, such as the approach reported by Meher et al. (2019), who have used Green's function to describe the response of a beam traversed by a traveling mass. Furthermore, the vibration control of beams, considering vehicle-bridge interaction, has been investigated by Pi & Ouyang (2016), and the critical speed of a traveling mass, affecting the behavior of the coupled mass-beam system, has been the focus of work by Dehestani et al. (2009). A recent work, reported by Abu-Alshaikh et al. (2020), has focused on obtaining analytical responses of a functionally graded beam with a traveling mass using Caputo-Fabrizio fractional derivative models.

Nevertheless, damage detection on beams with traveling masses has received scarce attention. An early approach has been proposed by Billelo & Bergman (2004), basing damage detection on comparing the displacement histories obtained from an intact bridge model before and after inducing damage. In recent work, Cicirello (2019) has studied the response bounds of Euler-Bernoulli beams with structural damage from a theoretical standpoint. Moreover, Zhan et al. (2021), have used wavelet transform coefficients of experimentally derived modal parameters for indirect damage detection. Despite the solid background offered by the aforementioned approaches, damage detection relies on either displacement measurements, which, although frequently used in experimental techniques, are uncommon in state-of-the-art SHM systems employed for structural maintenance, or on the accuracy of experimentally derived modal parameters, which is hardly guaranteed in non-stationary problems. As a result, damage detection on beams with traveling masses stands to benefit from an approach compatible with measurements typically collected in modern SHM systems (e.g. acceleration response data) and with state-of-the-art computational tools.

The non-stationarity of the traveling-mass problem calls for advanced data analysis methods, drawing from the field of artificial intelligence and its subset machine learning (ML), which has been employed in civil engineering applications, such as in fault diagnosis of SHM systems (Al-Zuriqat et al., 2023). In this direction, this paper presents a concept for damage detection on lightweight bridges with traveling masses, using a ML model for classifying acceleration response data into structural damage scenarios. The reasoning behind using ML is that damage patterns manifested in acceleration response data may be either too subtle to discern or obscured in frequency-domain representations of the data, due to the non-stationarity of the problem. The ML classification model, used in this study, is a convolutional neural network (CNN), which is trained with "labeled" acceleration response data, i.e. data corresponding to predefined structural condition scenarios, obtained from simulations using a well-calibrated analytical model. Upon completing training, classification is performed using real-world acceleration response data. The proposed concept is validated in preliminary laboratory tests, showcasing the capability of the CNN in identifying structural damage, as represented by partial loss of fixity at one support of a steel beam. The remainder of the paper includes a presentation of the concept, followed by the validation tests. The paper ends with a summary and conclusions and an outlook on future research.

Damage detection in lightweight bridges with traveling masses

The cornerstone of the proposed concept is the coupling between analytical modeling and simulation with ML. It is therefore clear that creating a well-calibrated analytical model for producing the acceleration response data for training the CNN is particularly important. As such, the description of the concept in this section starts with a brief discussion on the analytical modeling and simulation method employed for producing acceleration response data, followed by a presentation of the CNN training, including the preprocessing of the acceleration response data and the functionality of the CNN.

Analytical modeling of the traveling-mass problem

In its simplest form, a lightweight bridge with a traveling mass can be modeled as a continuous Euler-Bernoulli beam, as shown in Figure 1. The equation of motion of the beam accounts for inertia forces both of the vibrating beam and of the travelling mass (Dadoulis & Manolis, 2023):

$$\rho A\ddot{w}(x,t)+c\dot{w}(x,t)+EIw''''(x,t)=f_c\delta\left(x-|v|t\right). \quad (1)$$

In Equation (1), ρ is the material density, A is the cross-section area of the beam, E is the modulus of elasticity, I is the moment of inertia of the beam in the vertical direction, c is the damping coefficient, w is the vertical displacement of the neutral axis of the beam, δ is the Dirac delta, x represents the spatial coordinate in the longitudinal direction of the beam, and t is time. The functional $f_c > 0$ represents the contact force between the traveling mass and the beam, and $|v|$ is the speed of the traveling mass. Finally, $\dot{w} = \partial w/\partial t$, $\ddot{w} = \partial^2 w/\partial t^2$, and $w'''' = \partial^4 w/\partial x^4$.

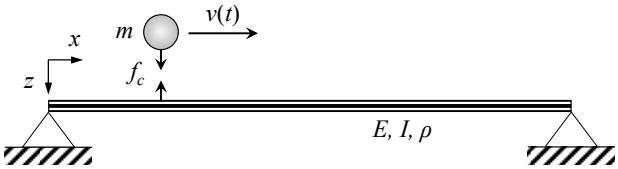

Figure 1: Bernoulli-Euler beam with traveling mass.

From Equation (1), it is evident that the factor that differentiates the traveling-mass problem from a regular Euler-Bernoulli-beam equation of motion is the contact force f_c. To estimate f_c, the equilibrium at the contact point of the traveling mass with the beam is considered. First, the static equilibrium is expressed as the total vertical displacement w_T, which is a summation of the vertical displacement of the beam and a component representing the surface roughness $r(x) = r(|v|t)$:

$$w_T\left(|v|t,t\right)=w\left(|v|t,t\right)+r\left(|v|t\right). \quad (2)$$

Furthermore, the dynamic equilibrium is provided by the following expression:

$$m\ddot{w}_T\left(|v|t,t\right)=mg-f_c, \quad (3)$$

where g is the gravitational acceleration. By solving Equations (2) and (3) with respect to f_c and by substituting f_c into Equation (1), the equation of motion is converted into:

$$\rho A\ddot{w}+c\dot{w}+EIw''''=m\left[g-\frac{d^2w}{dt^2}-\frac{d^2r}{dt^2}\right]\delta\left(x-|v|t\right). \quad (4)$$

In Equation (4), the time and spatial coordinate of w have been dropped for simplicity. It is noted that the right-hand side of Equation (4) includes total derivatives, which are expanded as follows:

$$\frac{d^2w}{dt^2}=\frac{\partial^2w}{\partial t^2}+2v\frac{\partial^2w}{\partial x\partial t}+v^2\frac{\partial^2w}{\partial x^2}, \quad (5)$$

$$\frac{d^2r(x)}{dt^2}=\frac{\partial^2r}{\partial x^2}\left(\frac{dx}{dt}\right)^2=v^2\frac{\partial^2r}{\partial x^2}. \quad (6)$$

In Equation (5), the second term corresponds to the Coriolis acceleration, and the third term is the centrifugal acceleration, which is irrelevant to the problem being studied and is therefore neglected. Using Equations (5) and (6), Equation (4) becomes:

$$\rho A\ddot{w} + c\dot{w} + EIw'''' = m\left[g - \ddot{w} - 2v\dot{w}' - v^2 r'' \right]\delta(u) \qquad (7)$$
$$u = x - vt.$$

Equation (7) is solved via modal analysis, for which the vertical displacement is analyzed into a spatial component and a temporal component:

$$w(x,t) = \varphi_n(x)\, q_n(t), \qquad n = 1,2,...,p\,, \qquad (8)$$

where $\varphi_n(x)$ is nth "eigenfunction", representing the mode of vibration in the form of a wave function, and $q_n(t)$ is the nth "generalized" coordinate function, which characterizes the temporal variation of the vibration. From Equation (8), it is clear that the complexity of the solution depends on the number of eigenfunctions (p) considered. For regular structures in structural dynamics, it is common to consider only a few eigenfunctions, which are capable of capturing the structural dynamic behavior. The nth eigenfunction is given by:

$$\varphi_n(x) = \sqrt{\frac{2}{\rho AL}} \sin\left(\frac{n\pi x}{L}\right), \qquad (9)$$

where L is the beam length. Eigenfunctions follow the orthogonality condition:

$$\rho A \int_0^L \varphi_i(x)\varphi_j(x)\,dx = \delta_{ij}\,, \qquad (10)$$

where δ_{ij} is the Kronecker delta. As a result, by substituting Equation (8) into Equation (7) for p eigenfunctions arranged in vector format $w = \boldsymbol{\varphi}(x)\mathbf{q}(t)$, ($\boldsymbol{\varphi}(x) = [\varphi_1(x),\varphi_2(x),\ldots,\varphi_p(x)]$, $\mathbf{q}(t) = [q_1(t),q_2(t),\ldots,q_p(t)]^T$), pre-multiplying with $\boldsymbol{\varphi}(x)^T$, integrating over L, and exploiting the Dirac delta property:

$$\int_0^L \varphi(x)\delta(x - vt)\,dx = \varphi(vt)\,, \qquad (11)$$

proven in Dadoulis & Manolis (2022), the equation of motion is recast into a $p \times p$ system of differential equations of the following format:

$$\begin{aligned}
&\mathbf{M}(t)\ddot{\mathbf{q}}(t) + \mathbf{C}(t)\dot{\mathbf{q}}(t) + \mathbf{K}(t)\mathbf{q}(t) = \mathbf{F}(t)\\
&\mathbf{M}(t) = \mathbf{I} + m\boldsymbol{\varphi}\boldsymbol{\varphi}^T\\
&\mathbf{C}(t) = diag(2\xi_n\omega_n) + 2mv\boldsymbol{\varphi}\boldsymbol{\varphi}'^T\\
&\mathbf{K}(t) = diag(\omega_n^2) + mv^2\boldsymbol{\varphi}\boldsymbol{\varphi}''^T\\
&\mathbf{F}(t) = mg\boldsymbol{\varphi} - mv^2 r''\left(x(t)\right)\boldsymbol{\varphi}.
\end{aligned} \qquad (12)$$

In Equation (12), ξ_n is the critical damping ratio of the nth eigenfunction, and ω_n is the respective natural frequency, computed as follows:

$$\xi_n = \frac{c}{2\rho AL\omega_n} \qquad \omega_n = \frac{n^2\pi^2}{L^2}\sqrt{\frac{EI}{\rho AL}}. \qquad (13)$$

For producing the structural response to the traveling-mass problem, the generalized coordinate functions $\mathbf{q}(t)$ need to be computed. To this end, Equation (12), which represents a set of ordinary differential equations of second order, is converted into a set of first-order ordinary differential equations, using the state-space formulation:

$$\dot{\mathbf{y}}(t) = \left[-\mathbf{A}^{-1}(t)\mathbf{B}(t)\right]\mathbf{y}(t) + \mathbf{A}^{-1}(t)\mathbf{h}(t)\,. \qquad (14)$$

The notations in Equation (14) are explained as follows:

$$\begin{aligned}
&\mathbf{A}(t) = \begin{bmatrix} \mathbf{0} & \mathbf{M}(t) \\ \mathbf{M}(t) & \mathbf{C}(t) \end{bmatrix},\ \mathbf{B}(t) = \begin{bmatrix} -\mathbf{M}(t) & \mathbf{0} \\ \mathbf{0} & \mathbf{K}(t) \end{bmatrix}\\
&\dot{\mathbf{y}}(t) = \begin{bmatrix} \dot{\mathbf{q}}(t) \\ \mathbf{q}(t) \end{bmatrix}, \qquad \mathbf{h}(t) = \begin{bmatrix} \mathbf{0} \\ \mathbf{F}(t) \end{bmatrix}.
\end{aligned} \qquad (15)$$

Assuming discrete time, Equation (14) is solved for every time instance k by performing eigenvalue analysis to matrix $(-\mathbf{A}_k)^{-1}\mathbf{B}_k$, which is non-symmetric and yields a matrix of complex eigenvalues $\boldsymbol{\Lambda}_k$ and eigenvectors matrix $\boldsymbol{\Psi}$. The eigenvalues matrix is given by:

$$\begin{aligned}
&\boldsymbol{\Lambda}_k = diag(\boldsymbol{\lambda}_{n,k}),\ \ \boldsymbol{\lambda}_{n,k} = \begin{bmatrix} e^{\lambda_{n,k}} & 0 \\ 0 & e^{\bar{\lambda}_{n,k}} \end{bmatrix},\\
&\lambda_{n,k} = \xi_{n,k}\omega_{n,k} \pm i\omega_{n,k}\sqrt{1-\xi_{n,k}^2}, \quad \xi_{n,k} \neq \xi_n.
\end{aligned} \qquad (16)$$

Using Equation (16), the solution of Equation (14) at time instance k is:

$$\begin{aligned}
&\mathbf{y}_k = \boldsymbol{\Theta}_k\left(\boldsymbol{\Theta}_{k-1}\right)^{-1}\mathbf{y}_{k-1} + \boldsymbol{\Theta}_k \int_{k-1}^{k} \left(\boldsymbol{\Theta}_s\right)^{-1}\mathbf{A}_k^{-1}\mathbf{h}_k\,ds\\
&\boldsymbol{\Theta}_k = \boldsymbol{\Psi}_k\boldsymbol{\Lambda}_k.
\end{aligned} \qquad (17)$$

The generalized coordinate functions are used together with the eigenfunctions to reconstruct the vertical displacement functions $w(x,t)$ using Equation (8). In turn, the vertical displacement functions are used as to produce the acceleration response data using Equation (14) (hereinafter termed "simulation data"), which are processed to be used for training the CNN.

Training of a convolutional neural network for damage detection

In theory, the simulation data could be used "as is" (i.e. in time-history format) as input to the CNN, since simulation data is relatively "clean" from noise and random components. However, upon completing training, the

CNN is expected to be applicable with real-world acceleration response data, in which the presence of spurious factors, such as noise and random components, is likely. As argued in Fritz et al. (2022), to reduce the effect of spurious factors and expose features in the simulation data, data preprocessing is necessary. Considering the non-stationarity of the traveling-mass problem, common preprocessing methods, producing fixed-window frequency-domain representations are hardly informative. Instead, preprocessing that depicts the coupled time-frequency content of the simulation data is necessary. Furthermore, as evidenced in Equation (14), the eigenvalues of the coupled traveling-mass-beam system change at every time instance k. As a result, a preprocessing method that enables tracking the evolution of eigenvalues is used, namely the Gabor transform (Qian & Chen, 1993):

$$G_w(\kappa) = S\left[\sum_{j=1}^{N} \ddot{w}(x,t_j)\, z_j e^{-i2\pi\kappa j/N}\right]^2, \kappa = \frac{N\cdot f}{f_s}. \quad (18)$$

In Equation (18), G_w is the Gabor coefficient, κ is the index of the discrete frequency bin of frequency f, considering a discrete set of simulation data of length N, sampled at frequency f_s ($f_s = 1/\Delta t$). The "Gabor" window function is denoted as z_j and could be any window function, such as the Gaussian function or the Hann window. Finally, S is a scaling factor.

Gabor coefficients are typically illustrated as colormap images. An exemplary illustration of a Gabor-transform image of simulation data representing acceleration of an Euler-Bernoulli beam is given in Figure 2.

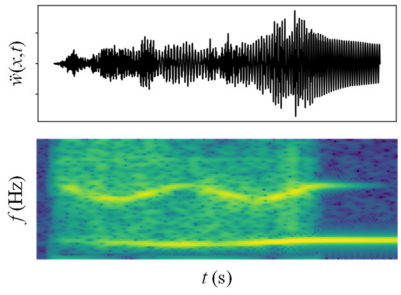

Figure 2: Gabor transform depiction of simulation data.

Upon producing the Gabor transform images, the damage detection problem is reduced to a classification problem, which is solved by the CNN. As shown Figure 3, a typical CNN consists of one *input* layer, a succession of *convolution* layers and *pooling* layers, (at least) one *fully-connected* layer, one *dropout* layer, and one *output* (classification) layer. Each Gabor transform image is passed in red-green-blue (RGB) format of size $N_I \times N_I \times 3$ from the input layer to the first convolution layer. Thereupon, the image is subjected to feature extraction, performed by progressively "sliding" square matrix "kernels" of size $n_I \times n_I \times 3$ (generally, $n_I << N_I$) over the image and by convolving RGB values of image areas (of dimensions matching the kernel size) with the kernel matrix elements. The outcome of each convolution layer is a so-called "feature map", consisting of convolutional products, and each product is fed to an activation function, which introduces non-linearity to the CNN, necessary for solving non-trivial problems. The outcomes of the activation function ("activations") are propagated to the pooling layer, which applies a sliding-window operation on the activations, typically computing either the average of each sliding window or the maximum value, to reduce the dimensionality of the activations. The last pooling layer is succeeded by a fully-connected layer, which comprises neurons connected to every outcome of the pooling layer. The fully-connected layer is followed by a dropout layer, in which a predefined percentage of features are "dropped" (i.e. ignored) to prevent overfitting. Finally, the dropout layer is connected to the output layer, which holds the classes.

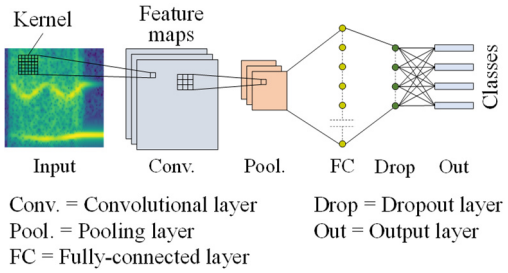

Figure 3: Layout of a typical CNN.

To perform classification, the CNN is trained, i.e. the kernels are fine-tuned so that the prediction accuracy of the output layer exceeds a predefined threshold. The training is performed using a "labeled" set of Gabor transform images, i.e. images that correspond to known structural conditions, including images from the intact structure as well as images from damage scenarios, simulated via perturbing structural parameters of the analytical model. The labeled set is divided into a training set, a validation set, and a testing set. The training set is propagated sequentially (in "batches") through the CNN, and the prediction error gradient, obtained from the output layer is back-propagated to update the kernels using an optimization algorithm, such as gradient descent, and a learning rate, which controls the fine-tuning rate of the kernels. Each cycle of propagation and back-propagation of a batch is a training iteration, and once all the images in the training set are used, one epoch is completed. The validation set is passed through the CNN periodically during training, after a predefined number of iterations. The purpose of validation is to monitor the prediction accuracy improvement of the CNN with an independent set of images so as to avoid overfitting the CNN to the training set. The testing set is passed through the CNN at the end of training, i.e. upon achieving the predefined prediction accuracy, to check the CNN performance.

A proof-of-concept implementation and validation of the proposed concept, including the analytical modeling of a beam structure, the data preprocessing and the training of

a CNN for damage classification are presented in the next section.

Implementation and validation

The prototype implementation and validation of the proposed concept involve defining software tools for simulations and CNN training, as well as devising a laboratory proof-of-concept test. In this section, first the implementation is discussed, followed by the presentation of the validation test and a discussion of the results.

Implementation

The first part of the implementation consists in developing an algorithm for analytical modeling and data pre-processing, based on Equations (1)-(18). The algorithm is written in the Python programming language and consists of functions *model_setup*, *eig_decomp* and *state_space_comp*, dedicated to (i) computing the matrices **A** and **B** for every time instance k, (ii) performing eigenvalue analysis to matrix $(-\mathbf{A}_k)^{-1}\mathbf{B}_k$, and (iii) to applying Equation (17) to compute the vector $\mathbf{y}_k$, respectively. A separate function, *data_gen*, is written to retrieve the displacement histories, using the eigenfunctions, and to compute the acceleration response data using Equation (14). Finally, the Gabor transform is realized by function *gaborTrsf*, and the corresponding images are produced.

The second part of the implementation involves developing and training the CNN. Since, only a proof-of-concept study is shown, an elaborate parametric analysis of the CNN performance and an optimal definition of the CNN architecture fall beyond the scope of this paper and will be investigated in future research. Instead, the MATLAB deep learning tool is leveraged, and a simple CNN architecture is devised, shown in Figure 4, adjusted to the input of Gabor transform images and to the number of classes being considered.

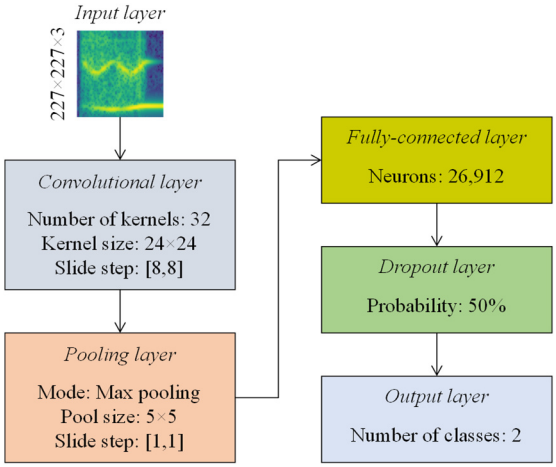

Figure 4: The CNN architecture defined in this study.

Validation tests

The laboratory validation test is devised on a simply supported HEB100 steel beam, representing a downscaled model of a lightweight bridge traversed by a traveling mass, shown in Figure 5. The cross section of the beam has dimensions 100×100×10×6 (mm) (width × height × flange thickness × web thickness). The total length of the neutral axis of the beam is 5830 mm. The beam is part of an experimental setup, which includes adjustable struts that ensure that the beam is level. It is noted that the beam is supported only at its ends, i.e. the struts are not used as supports to the beam. The experimental setup also consists of pulleys that enable masses to move along the longitudinal axis of the beam and a motor that controls the mass speed.

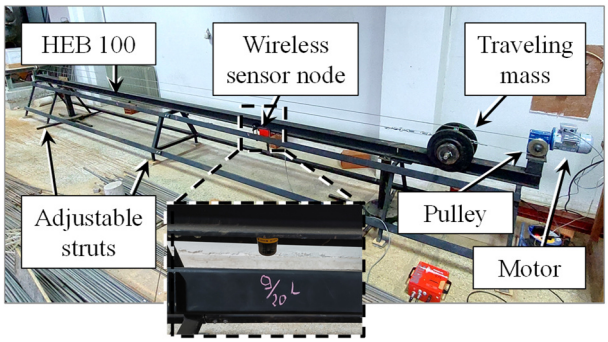

Figure 5: Experimental setup.

An analytical model of the beam is developed and used for simulating the motion of a traveling mass across the beam. The modulus of elasticity and the material density are computed via preliminary laboratory tests as $E = 198.5$ GPa and $\rho = 7.65 \cdot 10^3$ kg/m^3, respectively. To produce a labeled set covering a sufficient part of the available solutions space, the mass value and speed are randomly perturbed to devise several simulation scenarios. Specifically, the mass (m) assumes values between 10 kg and 40 kg, and the speed ($|v|$) assumes values between 0.2 m/s and 0.5 m/s. With respect to the structural condition, two structural "states" are considered, one for the intact beam and one assuming loss of fixity at one support, i.e. by substituting the vertical support with a translational spring. A total of 500 simulations are conducted for each state, computing acceleration response data at a distance equal to $9L/20$ from the beam end and at a sampling frequency of $f_s = 128$ Hz. The reasoning behind avoiding the midspan of the beam is that the second eigenfunction, which contributes to the structural response, is characterized by an antisymmetric sinusoidal shape with a zero-crossing point at the midspan. Hence, collecting acceleration response data from the midspan would underestimate the contribution of the second eigenfunction. In turn, 500 Gabor transform images per class are produced, forming the labeled set used for training the CNN. Exemplary illustrations of Gabor transform images for both states are given in Figures 6 and 7. The variation of the first two eigenfrequencies is marked for both structural states considered, as a result of the variable structural dynamic properties of the beam due to the motion of the mass. As can be seen in the figures, the loss of fixity at the support

reduces the eigenfrequencies; however, the variation trend is similar in both states.

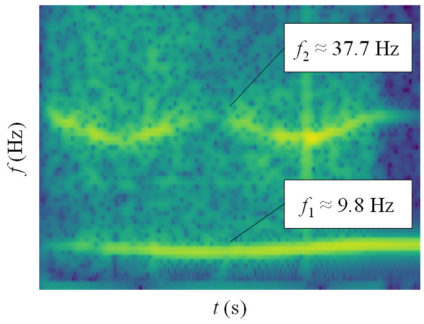

Figure 6: Gabor transform for the intact beam (m = 23.3 kg, $|v|$ = 0.351 m/s).

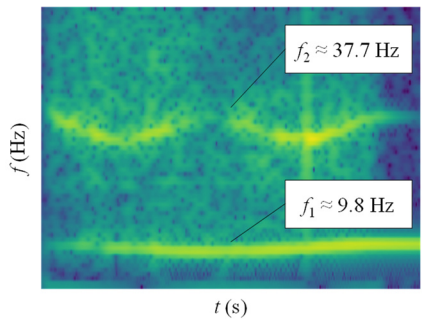

Figure 7: Gabor transform for the damaged beam (m = 15 kg, $|v|$ = 0.46 m/s).

The training of the CNN is performed by first splitting the labeled set into 70% training set (350 images), 20% validation set (100 images), and 10% testing set (50 images). During training, the "Adam" optimizer – a stochastic gradient-descent optimization algorithm – is employed for fine-tuning the kernels in each iteration (Kingma & Ba, 2015). The initial learning rate is set to 0.001, the batch size is 30 images, and the validation frequency is defined at every 30 iterations. The total number of epochs is set equal to 10, and the learning rate is reduced at every epoch by a factor of 0.5. A high training accuracy of 98% is achieved after 122 iterations, and the accuracy of the validation set reaches 100% after 30 iterations, as shown in Figure 8.

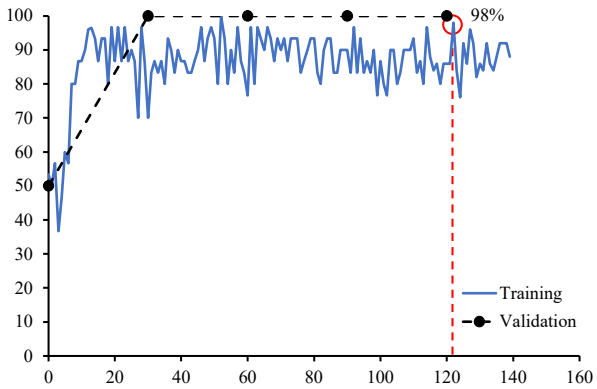

Figure 8: Training and validation accuracy history.

Prior to applying the CNN with acceleration response data from the experimental setup, the classification capability of the CNN is verified using the testing set. The classification test results are given below in the form of a "confusion" matrix:

Table 1: Confusion matrix for the testing data set.

	Intact	Damaged
Intact	50	0
Damaged	0	50

The results for the testing dataset corroborate the training accuracy, since every image of the testing dataset has been correctly classified. The next step of the validation test involves using the CNN for classifying Gabor transform images produced from real-world acceleration response data obtained from the experimental setup. The data is collected using a Lord Microstrain G-Link-200 wireless sensor node capable of measuring acceleration in 3 axes at ranges up to ±8g and at sampling frequencies up to 4,096 Hz (Microstrain Sensing, 2020). Experiments are conducted for two structural states, matching the states used in the simulations, using 30 combinations of mass and speed values per state, as listed in Table 2.

Table 2: Combinations of mass and speed values for the laboratory experiments.

Nr.	**Mass** m (kg)	**Speed** $\|v\|$ (m/s)	**Nr.**	**Mass** m (kg)	**Speed** $\|v\|$ (m/s)
1	13	0.25	16	27	0.40
2	13	0.30	17	27	0.45
3	13	0.35	18	27	0.50
4	13	0.40	19	18	0.25
5	13	0.45	20	18	0.30
6	13	0.50	21	18	0.35
7	23	0.25	22	18	0.40
8	23	0.30	23	18	0.45
9	23	0.35	24	18	0.50
10	23	0.40	25	38	0.25
11	23	0.45	26	38	0.30
12	23	0.50	27	38	0.35
13	27	0.25	28	38	0.40
14	27	0.30	29	38	0.45
15	27	0.35	30	38	0.50

The loss of fixity is realized by placing a spring between the beam end and its support. Acceleration response data is collected for every experiment close to the midspan of the beam, at a point located at 9L/20 from the beam end, as shown in Figure 5, at a sampling frequency of f_s = 128 Hz, as in the simulations. The acceleration response data from each experiment is used to produce a Gabor transform image, resulting in a set of 60 Gabor transform images to be fed to the CNN, an example of which is shown in Figure 9.

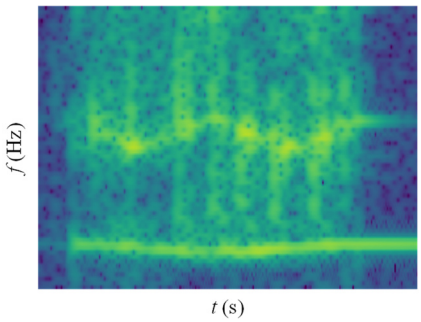

Figure 9: Gabor transform for experiment 10 (intact beam).

The similarity between Figure 9 and Figures 6 and 7 is indicative of the satisfactory proximity between the analytical model and the experimental setup. The Gabor transform images are fed to the CNN and classified into the two classes, corresponding to the states considered. The results are summarized in the following confusion matrix:

Table 3: Confusion matrix for the experiments.

	Intact	Damaged
Intact	30	0
Damaged	1	29

The results of the experiments clearly highlight the capability of the CNN to correctly classify real-world acceleration response data. From the Gabor transform images of the intact beam, only one experiment is misclassified as "damaged", while the respective images of the damaged beam are all correctly classified. Furthermore, the results serve as proof of the validity of the proposed concept and of the "transferability" of the CNN training from the domain of simulations to the real world.

Summary and conclusions

Damage detection on lightweight bridges with traveling masses is a non-stationary problem that is hardly covered by conventional methods, developed for experimental testing or structural health monitoring. In this context, this paper has presented a concept towards detecting damage on lightweight bridges, represented by Euler-Bernoulli beams. The proposed concept is based on analyzing the behavior of the beam using analytical modeling for a set of predefined damage scenarios and on using simulation-derived acceleration response data to train a convolutional neural network to classify the data into the damage scenarios. Thereupon, the convolutional neural network is applied using real-world acceleration response data.

The proposed concept has been validated in a proof-of-concept laboratory test on a steel beam with a traveling mass, representing a downscaled model of a lightweight bridge. The results have shown that the convolutional neural network (i) can be trained with high accuracy using simulation-derived acceleration response data and (ii) can be transferred to real-world applications, assuming adequate calibration of the analytical model. Future work may focus on considering several damage scenarios, anticipated to occur over the lifetime of lightweight bridges, as well as on developing the proposed concept into a structural health monitoring approach.

Acknowledgments

This paper is the result of a collaborative effort of authors funded by different sources. The authors would like to gratefully acknowledge the support offered by the German Research Foundation (DFG) under grant SM 281/20-1, by the Hellenic Foundation for Research and Innovation (HFRI) under grant 6255, as well as by the German Federal Ministry for Digital and Transport (BMDV) within the mFUND program under grant 19FS2013B. Results presented in this work have been produced using the Aristotle University of Thessaloniki High-Performance Computing Infrastructure. Any opinions, findings, conclusions, or recommendations expressed in this paper are those of the authors and do not necessarily reflect the views of the DFG, the HFRI, or the BMDV.

References

Abu-Alshaikh, I.M. & Almbaidin, A.A. (2020). Analytical responses of functionally graded beam under moving mass using Caputo and Caputo–Fabrizio fractional derivative models. Journal of Vibration and Control, 26(19-20), pp. 1859-1867.

Al-Zuriqat, T., Chillón Geck, C., Dragos, K., & Smarsly, K. (2023). Adaptive fault diagnosis for simultaneous sensor faults in structural health monitoring systems. Infrastructures, 8(3), 39.

Bilello, C. & Bergman, L.A. (2004). Vibration of damaged beams under a moving mass: theory and experimental validation. Journal of Sound and Vibration, 274(3-5), pp. 567-582.

Cicirello, A. (2019). On the response bounds of damaged Euler–Bernoulli beams with switching cracks under moving masses. International Journal of Solids and Structures, 172-173(2019), pp. 70-83.

Dadoulis, G. & Manolis, G.D. (2022). On the detection of fracture within vibrating beams traversed by a moving force. Infrastructures, 7(7), 93.

Dadoulis, G. & Manolis, G.D. (2023). Dynamic response of a damaged bridge model traversed by a heavy point mass. Journal of Sound and Vibration, 551(2023), 117613.

Dallard, P., Fitzpatrick, T., Flint, A., Low, A., Ridsdill Smith, R., Willford, M., & Roche, M. (2001). London Millennium Bridge: Pedestrian-induced lateral vibration. ASCE Journal of Bridge Engineering, 6(6), pp. 412-417.

Dehestani, M., Mofid, M., & Vafai, A. (2009). Investigation of critical influential speed for moving mass problems on beams. Applied Mathematical Modeling, 33 (2009), 3885-3895.

Dragos, K., Magalhães, F., Manolis, G. D., & Smarsly, K. (2024). Frequency-domain synchronization of structural health monitoring data. Journal of Sound and Vibration, 571(2024), 118017.

Firus, A. (2023). A contribution to moving force identification in bridge dynamics. Wiesbaden, Germany, Springer Vieweg.

Flaga, K. (2000). Advances in materials applied in civil engineering. Journal of Materials Processing Technology, 106(1-3), pp. 173-183.

Fritz, H., Peralta, J., Legatiuk, D., Steiner, M., Dragos, K., & Smarsly, K. (2022). Fault diagnosis in structural health monitoring systems using signal processing and machine learning techniques. In: Cury, A., Ribeiro, D., Ubertini, F., Todd, M. D. (eds.). Structural health monitoring based on data science techniques. Pp. 143-164. Cham, Switzerland: Springer.

Kingma, D.P. & Ba, J. (2015). Adam: A method for stochastic optimization. In: 3rd International Conference on Learning Representations, San Diego, CA, USA, 05/07/2015.

Meher, S., Parida, S., & Behera, R.K. (2019). On the response of a beam structure to a moving mass using Green's function. In: 1st International Conference on Applied Mechanical Engineering Researh. Waragnal, India, 05/02/2019.

Microstrain Sensing, 2020. Microstrain Sensing product datasheet: G-Link-200. Williston, VT, USA: Parker Hannifin Corp.

Pi, Y. & Ouyang, H. (2016). Vibration control of beams subjected to a moving mass using a successively combined control method. Applied Mathematical Modeling, 40(2016), pp. 4002-4015.

Qian, S. & Chen, D. (1993). Discrete Gabor transform. IEEE Transactions on Signal Processing, 41(7), pp. 2429-2438.

Siddiqui S.A., Golnaraghi, M.F., & Heppler, G.R. (1998). Dynamics of a flexible cantilever beam carrying a moving mass. Nonlinear Dynamics, 15(1998), pp. 137-154.

Zhan, Y., Au, F.T.K., & Zhang, J. (2021). Bridge identification and damage detection using contact point response difference of moving vehicle. Structural Control Health Monitoring, 28(12), e2837.

Zhang, Z., Mehmood, A., Shu, L., Huo, Z., Zhang, Y., & Mukherjee, M. (2018). A survey on fault diagnosis in wireless sensor networks. IEEE Access, 6(2018), pp. 11349-11364.

Zhang, Z., Yuvaraj, A., Di, J., & Qian, S. (2019). Matrix design of light weight, high strength, high ductility ECC. Construction and Building Materials, 210(2019), pp. 188-197.